

PCCP

Physical Chemistry Chemical Physics

Accepted Manuscript

This article can be cited before page numbers have been issued, to do this please use: M. Witwicki, A. Lewiska and A. Ozarowski, *Phys. Chem. Chem. Phys.*, 2021, DOI: 10.1039/D1CP01596F.



This is an Accepted Manuscript, which has been through the Royal Society of Chemistry peer review process and has been accepted for publication.

Accepted Manuscripts are published online shortly after acceptance, before technical editing, formatting and proof reading. Using this free service, authors can make their results available to the community, in citable form, before we publish the edited article. We will replace this Accepted Manuscript with the edited and formatted Advance Article as soon as it is available.

You can find more information about Accepted Manuscripts in the [Information for Authors](#).

Please note that technical editing may introduce minor changes to the text and/or graphics, which may alter content. The journal's standard [Terms & Conditions](#) and the [Ethical guidelines](#) still apply. In no event shall the Royal Society of Chemistry be held responsible for any errors or omissions in this Accepted Manuscript or any consequences arising from the use of any information it contains.

ARTICLE

o-Semiquinone radical anion isolated as an amorphous porous solid†‡

Maciej Witwicki,^{*a} Agnieszka Lewińska^a and Andrew Ozarowski^bReceived 00th January 20xx,
Accepted 00th January 20xx

DOI: 10.1039/x0xx00000x

The use of metal cations is a commonly applied strategy to create $S > \frac{1}{2}$ stable molecular systems containing semiquinone radicals. Persistent mono-semiquinonato complexes of diamagnetic metal ions ($S = \frac{1}{2}$) are hitherto less common and mostly limited to the complexes of heavy metal ions. In this work a mono-semiquinonato complex of aluminum, derived from 1,2-dihydroxybenzene, is obtained in a surprisingly short and uncomplicated procedure. The isolated product is an amorphous, porous solid that exhibits very good stability under ambient conditions. To characterise its molecular and electronic structure 9.7, 34 and 406 GHz EPR spectroscopy was used in concert with computational techniques (DFT and DLPNO-CCSD). It was revealed that the radical complex composes of two chemically equivalent aluminum cations and two catechol-like ligands with the unpaired electron uniformly distributed between the two organic molecules. The good stability and porous structure provide possibilities for the complex's applications in heterogeneous aerobic reactions.

Introduction

In 1900, Professor Moses Gomberg discovered that carbon can exist in a trivalent state¹ and since then organic radicals have been drawing the attention of researchers because of their reactivity and importance in understanding electronic structure and chemical bonding^{2–14}. Nowadays, radicals play an increasingly important role in modern material science^{15,16}. They have been used to produce high-spin metal complexes¹⁷, metal complexes with the single molecular magnet (SSM) behavior^{18,19} as well as purely organic molecular magnets and batteries^{16,20}. Many experiments have showed that the quantum efficiency of luminescence can be high for organic radicals^{21–24}. All in all, these open-shell molecules exhibit properties for a vast array of applications, e.g. in spintronics, bistable memory devices, sensing materials, organic LEDs or organic semiconductors^{15,16,25–27}. This study aims to contribute to the growing area of radical materials by bringing to the attention an o-semiquinone complex of Al^{3+} that is a porous material.

Semiquinones (sq) are typical organic radical anions being the intermediate form in the redox equilibrium between quinones and hydroquinones (Fig. 1). As radicals, they are unstable, but their stability can be tailored. Extensive research has shown that to lower the reactivity of radicals, one can either

sterically block the active spin sites with bulky groups or make the spin density significantly delocalised on the molecular frame^{15,28}. However, o-semiquinones can be also isolated as ligands in metal complexes and many o-semiquinonato complexes of paramagnetic d-electron metal ions have been synthesized^{17,29–34}. It is important to notice that in these compounds the radicals are additionally stabilised by the exchange interaction. This effect was also used to isolate *bis*- ($S = 1$) and *tris*-semiquinonato ($S = 3/2$) complexes of diamagnetic metals, e.g. $\text{Mg}(\text{sq})_2$, $\text{Al}(\text{sq})_3$ or $\text{Ga}(\text{sq})_3$ ^{35–39}. However, persistent *mono*-semiquinonato ($S = \frac{1}{2}$) complexes of diamagnetic metal ions are hitherto less common and mostly limited to the complexes of heavy metal ions that can form strong coordination bonds with these radical ligands^{40–43}. On this basis, we hypothesised that the increasing strength of chelation of a light and redox stable metal cation can protect the radical from reduction/oxidation. In the Pearson hard and

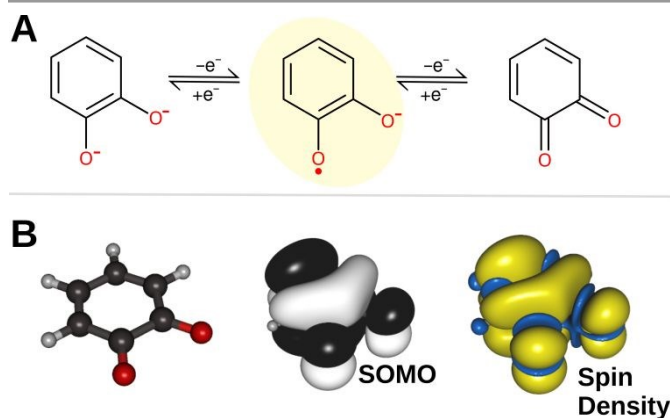


Fig. 1 The redox equilibrium between quinones and hydroquinones (A) along with the singly-occupied molecular orbital (SOMO) and the spin density for o-semiquinone radical (B).

^a Faculty of Chemistry, Wrocław University, Joliot-Curie 14, 50-383 Wrocław, Poland, maciej.witwicki@chem.uni.wroc.pl

^b National High Magnetic Field Laboratory, Florida State University, 1800 East Paul Dirac Drive, Tallahassee, FL 32310, United States

† Dedicated to Professor Adam Jezierski on the occasion of his honourable retirement

‡ Electronic Supplementary Information (ESI) available: Selected details of theoretical calculations, selected figures and tables. See

DOI: 10.1039/x0xx00000x

soft acids and bases concept, semiquinones can be labelled as a hard base and thus their stability should rise in a complex with small and highly charge cation like Al^{3+} .

Results and discussion

From the reaction mixture containing aluminium chloride hexahydrate, catechol (*o*-dihydroxybenzene) and iodine, a dark blue product (**1**) was isolated. **1** was soluble in water and alcohols, slightly soluble in DMSO, and insoluble in common aprotic organic solvents, namely THF, acetone, diethyl ether, chloroform, dichloromethane, pentane and toluene.

To confirm the radical character of **1** the EPR spectrum of its methanol solution was recorded at ~ 9.7 GHz at room temperature. This spectrum is composed of eleven resonance lines with relative intensity 1:2:3:4:5:6:5:4:3:2:1 and differs distinctly from the spectrum recorded for the uncomplexed radical anion of catechol (Fig. 2). For the latter the observed splitting is due to the hyperfine interaction of the unpaired electron with two nonequivalent pairs of the benzoic ring protons (Table 1). The number of lines and their relative intensity observed for **1** can result only from hyperfine interaction of the unpaired electron with two chemically equivalent nuclei of $I = 5/2$ and thus strongly indicates that **1** is a paramagnetic complex being an aluminium dimer (^{27}Al : $I = 5/2$, abundance 100%). The formation of aluminium dimers in the

presence of diamagnetic catechol-like ligands was reported^{44,45}. However, there is another possibility. Iodine (^{127}I : $I = 5/2$, abundance 100%) was used as an oxidising agent and thus iodine atoms might have been incorporated into the structure of **1** through iodination of catechol. This was excluded as EDX spectroscopy coupled with SEM did not reveal iodine atoms in **1**. Moreover, the synthesis carried out with hydrogen peroxide used as an oxidising agent instead of I_2 yielded the same blue product confirming that the eleven resonance lines originate from hyperfine interaction with two chemically equivalent ^{27}Al nuclei. This EPR spectrum was successfully simulated assuming $g_{\text{iso}} = 2.00367$ and $a_{\text{Al}} = 2.5$ MHz.

To the best of our knowledge, the first account of Al^{3+} complex with *o*-semiquinone radical was provided by Eaton⁴⁶, but that complex was not reported as containing two Al^{3+} ions and was not isolated as a stable product. The hyperfine coupling due to ^{27}Al observed by Eaton (1.96 Gs \approx 5.5 MHz) was more than twice the value we observed for **1**. The difference in the a_{Al} values strongly shows substantial structural dissimilarities between these two radical species.

Attempts to obtain **1** as crystalline material by crystallisation from various solvents and their mixtures remained unsuccessful, but the elemental analysis closely corresponded

Table 1 Summary of EPR measurements. The EPR spectra not shown in the text are given as ESI†

frequency	details	parameter	value	
Complex 1				
9.7 GHz	in methanol, 298 K	g_{iso}	2.00367	
		a_{Al}	2.5 MHz	
34 GHz	in methanol, 77 K	g_{eff}	2.00338	
	powder, 77 K	g_{eff}	2.00338	
	powder, 100 K	g_x	2.00485	
		g_y	2.00365	
		g_z	2.00210	
		g_{avg}	2.00350	
406.4 GHz	in methanol, 50 K	g_x	2.00454	
		g_y	2.00373	
	powder, 10 K	g_z	2.00203	
		g_{avg}	2.00343	
		g_x	2.00455	
		g_y	2.00377	
		g_z	2.00204	
		g_{avg}	2.00338	
	Uncomplexed radical			
	9.7 GHz	in methanol, 298 K	g_{iso}	2.00469
		a_{H1}	10.3 MHz	
		a_{H2}	2.1 MHz	
406.4 GHz	in methanol, 77 K	g_{eff}	2.00470	
	in methanol, 10 K	g_x	2.00573	
		g_y	2.00534	
		g_z	2.00233	
		g_{avg}	2.00447	

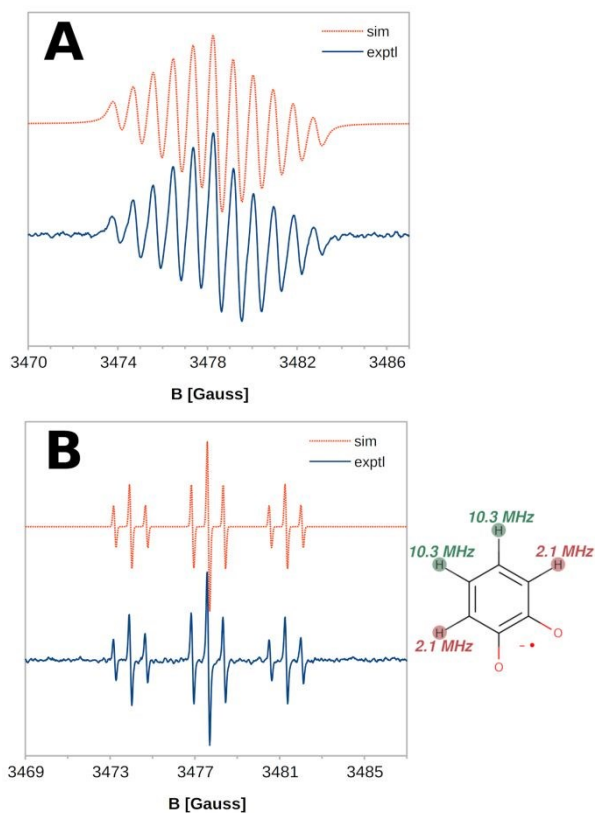


Fig. 2 Liquid phase (solution in methanol) EPR spectra recorded at 9.7 GHz (X-band) for radical complex **1** (A) and uncomplexed *o*-semiquinone radical derived from catechol (B).

to the formula of $\text{Al}_2(\text{C}_6\text{H}_4\text{O}_2)_2\text{Cl}_3(\text{H}_2\text{O})_6$ (found: C 29.22%, H 4.71%, Cl 22.53%, calcd. C 29.74%, H 4.16%, Cl 21.95%). According to thermogravimetric analysis (TGA, Fig. S1, ESI†), **1** is thermally stable up to 431 K (158 °C) with the onset point phase transition starting at 316 K (43 °C). The X-ray diffraction experiment (Fig. S2, ESI†) did not expose any crystallinity and differential scanning calorimetry (DSC) did not reveal peaks in heating and cooling (Fig. S3, ESI†), which combined strongly indicates an amorphous material⁴⁷. This stays in line with SEM micrographs (Fig. 3) showing that **1** is composed of irregularly shaped clumps that form cavities. The clumps contain pores with the upper limit in diameter being 1.2 μm (Fig. S4E and S4F, ESI†). According to the multiple point BET(N_2) results, the specific surface area (S_{BET}) of **1** is significant and amounts to 155.89 $\text{m}^2 \text{g}^{-1}$ whilst the pore volume to 0.16 $\text{cm}^3 \text{g}^{-1}$. This result is comparable with commercially available silica (Merc/Sigma Aldrich, area 175–225 $\text{m}^2 \text{g}^{-1}$) and porous silicon (PSi) widely applied in energy storage devices (304 and 328 $\text{m}^2 \text{g}^{-1}$ for PSi prepared from SiO and d-SiO). Fig. S5, ESI† presents N_2 adsorption isotherm for **1**. The isotherm is of type IV and shows a clear hysteresis loop at p/p_0 of 0.9 with the tail extending towards the lower limit of adsorption-desorption hysteresis. Such a shape of the loop indicates the occurrence of both open and constricted mesopores within a material as discussed in ref. 48.

The EPR parameters determined from the isotropic EPR spectrum shown in Fig. 2A are a source of structural information. However, the isotropic EPR spectrum composed of 11 lines can be observed for an aluminium dimer with one o-semiquinonate and one catecholate ligand ($S = 1/2$; $[\text{Al}_2(\text{sq})(\text{cat})]^{3+}$) or with two o-semiquinonate ligands ($S = 1$; $[\text{Al}_2(\text{sq})(\text{sq})]^{4+}$) in high exchange regime ($|J| \gg |A|$)^{49,50}. To conclusively differentiate between these two possibilities, the variable-temperature measurements of magnetic susceptibility were performed for **1**. The gram-susceptibility was converted to the molar susceptibility (χ_M) using the molar mass 484.6 g/mol

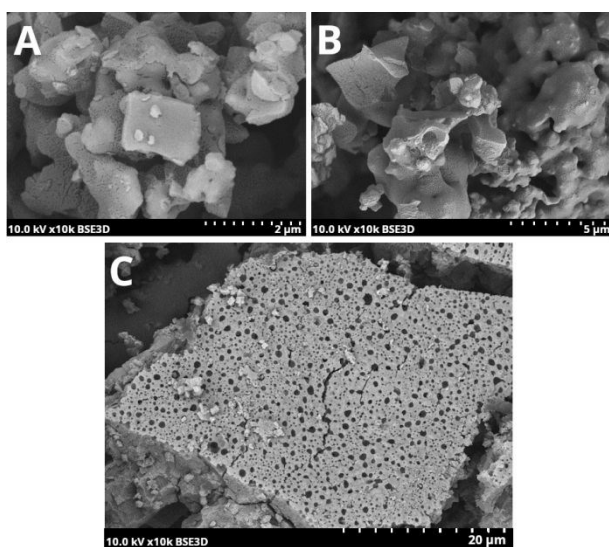


Fig. 3 SEM micrographs presenting cavities and pours of **1** at three different magnifications. Larger size images are gives as ESI† (Fig. S7) along with micrographs showing the diameters of pours.

corresponding to $\text{Al}_2(\text{C}_6\text{H}_4\text{O}_2)_2\text{Cl}_3(\text{H}_2\text{O})_6$. The temperature dependence of the product $\chi_M T$ is presented in Fig. 4 ($\chi_M = f(T)$ and $1/\chi_M = f(T)$ in Fig. S6A, ESI†). At room temperature, the product $\chi_M T$ amounts to 0.362 $\text{cm}^3 \cdot \text{K} \cdot \text{mol}^{-1}$. This value is close to what is expected for an uncorrelated $S = 1/2$ and $g \approx 2.0$ spin system (0.375 $\text{cm}^3 \cdot \text{K} \cdot \text{mol}^{-1}$), hence proves that **1** is a monoradical complex. From 50 to 300 K, the value of $\chi_M T$ remains nearly constant. Upon cooling below 50 K, the $\chi_M T$ decreases more markedly down to 0.248 $\text{cm}^3 \text{K mol}^{-1}$ at 2 K, indicating weak intermolecular antiferromagnetic coupling between the $S = 1/2$ complexes. A fit of the data to the Curie law with interaction of neighbouring spins treated as a molecular field correction (all symbols have their usual meaning)^{51,52}:

$$\chi'_M = g^2 \beta_e^2 N S (S+1) / (3kT)$$

$$\chi_M = \chi'_M \left[1 - \frac{2\chi'_M}{g^2 \beta_e^2 N} zJ' \right]$$

afforded the parameter $zJ' = 0.91 \text{ cm}^{-1}$ that corroborates the weak intermolecular antiferromagnetic interactions. In the fitting $g = 2.00367$ determined form EPR experiments was assumed and correction factor of 0.978 was used to account for a small amount of diamagnetic impurity. A number of studies have examined the magnetic susceptibility for radical systems with paramagnetic behaviour by fitting the experimental data to the Curie-Weiss law. For example, the small negative Weiss constant (θ), which is characteristic of weak antiferromagnetic interaction, of -2.2, -0.3 and -0.7 K was determined for 1,2,4-benzotriazinyl⁵³, 3-tert-butyl-1-phenyl-1,2,4-benzotriazinyl⁵⁴ and the Finland trityl radical⁵⁵, respectively. For comparison, we fitted $\chi_M T$ for **1** to the Curie-Weiss law (Fig. S6B, ESI†). Although this fit was less satisfactory, the determined value $\theta = -0.89 \text{ K}$ stays in line with findings for the above mentioned $S = 1/2$ radical systems.

The $S = 1/2$ nature of **1** is also supported by the spin concentration estimated by quantitative EPR. For **1** it was 1.0×10^{21} spin/g, which is reasonably close to the value of 1.24×10^{21} spin/g expected for $\text{Al}_2(\text{C}_6\text{H}_4\text{O}_2)_2\text{Cl}_3(\text{H}_2\text{O})_6$ with one o-semiquinonate and one catecholate ligand. Regarding these

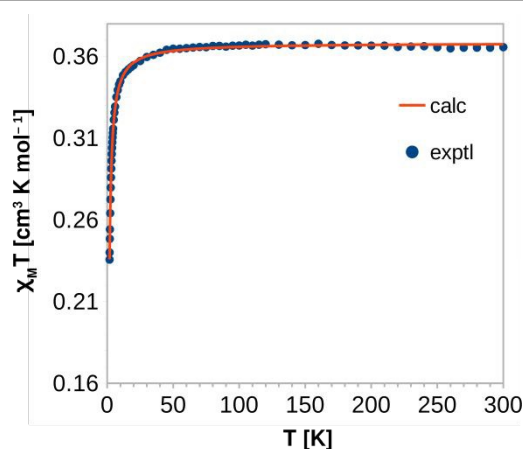


Fig. 4 Temperature dependence of $\chi_M T$ for **1**. The orange line corresponds to a fit to the Curie law with interaction of neighbouring spins treated as a molecular field correction ($g = 2.00367$, $zJ' = 0.91 \text{ cm}^{-1}$).

quantitative EPR measurements, some limitations need to be acknowledged. In estimating spin concentrations, the unknown sample and the quantitative standard should have similar characteristics, inter alia bulk dielectric constant, line shape, line width, power saturation characteristics and similar number of spin⁵⁶. This was impossible to completely fulfil for the new complex **1**.

The observed hyperfine splitting $a_{Al} = 2.5$ MHz confirms that the spin density is uniformly distributed between two aluminium atoms. Nevertheless, the a_{Al} value for **1** is very low for a nucleus ²⁷Al. It is lower from its already mentioned counterpart reported by Eaton⁴⁶ and from the hyperfine coupling constant determined for AlO (776 MHz)⁵⁷, for which spin density on the aluminium atom is high (~65% according to our previous CCSD/IGLO-III calculations⁵⁸). Therefore, the a_{Al} value shows that in **1** only a small fraction of spin density is on the aluminium atoms.

The a_{Al} value can be used to estimate the s-type spin population on aluminium atoms. The magnitude of isotropic hyperfine interaction constant for nucleus X (a_X) is proportional to the spin density at the nucleus X (ρ_X), which stems from the s orbitals spin population. This relation is described by the Fermi contact term:

$$a_X = (8\pi/3) g \beta_e g_X \beta_X \rho_X$$

Therefore, using the value of the isotropic hyperfine coupling constant for a paramagnetic aluminium atom with 100% spin population in an s orbital ($a_0 = 1395.5$ Gs⁴⁹ $\approx 3.9 \times 10^3$ MHz), the s-type spin population can be estimated as a_{Al}/a_0 . It was found for **1** to be only 0.064%. This result implies that the π -type singly-occupied molecular orbital (SOMO) of the radical (shown in Fig. 1) is not engaged in the covalent interaction with 2s orbitals of the aluminium atoms. Moreover, it implicitly excludes the covalent interaction between the SOMO and the aluminium's 2p orbitals as this would introduce significant spin population on aluminium atoms and bring about greater a_{Al} value because of the spin polarisation of the aluminium atoms' 1s orbitals.

What is interesting about the isotropic EPR spectra of **1** is that the hyperfine interaction due to ¹H nuclei is not observed. This is consistent with the report of Eaton⁴⁶, who also did not observe the hyperfine interaction due to ¹H. The lack of the ¹H splitting for **1** can be attributed to the significant delocalisation of the unpaired electron on the molecular frame. If one unpaired electron is delocalised on two organic ligand, then the hyperfine splitting constants due to ¹H, which are governed by spin polarisation mechanism⁵⁰, are expected to decrease noticeably even to where the lines due to these interactions remain unresolved and bring about inhomogeneous broadening. As shown in Fig. 2, the lines for **1** are noticeably wider in comparison with the uncomplexed radical, that is 0.45 and 0.08 G, respectively; the values are given as the distances between the inflection points.

To better understand the molecular and electronic structure of **1**, we attempted to determine the principle components of the **g** matrix (**g** tensor), namely g_z , g_y , g_x . EPR spectra for solid phase (powder and frozen methanol solution) were recorded at 9.7 GHz (X-band), 34 GHz (Q-band) and 406 GHz frequency

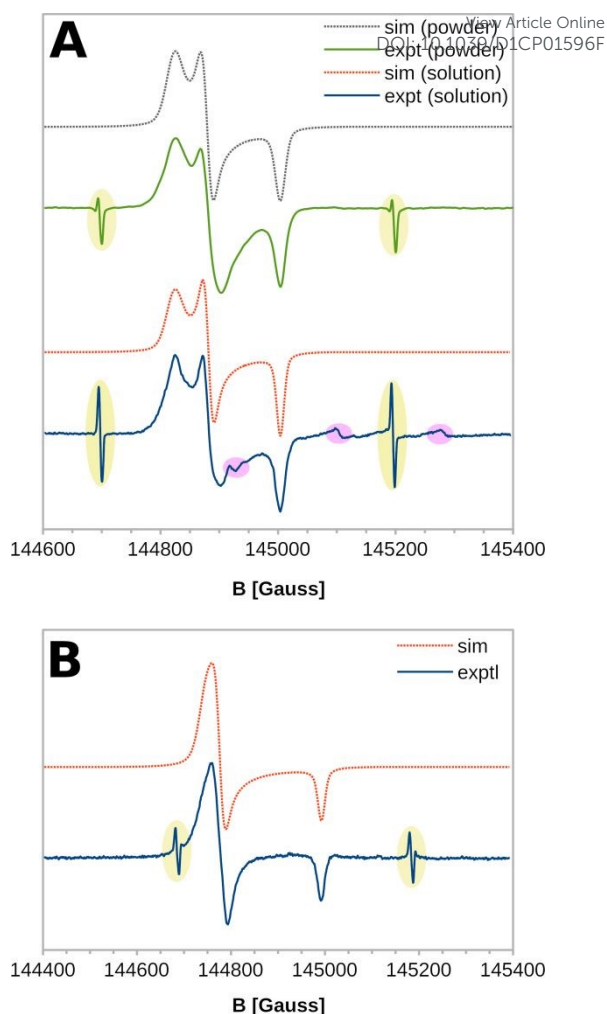


Fig. 5 Solid phase EPR spectra recorded at 406.4 GHz for: (A) radical complex **1** [powder at 10 K (green) and frozen methanol solution at 50 K (blue)]; (B) uncomplexed o-semiquinone radical derived from catechol (methanol solution at 10 K). Signals due to atomic hydrogen trapped in octaisobutylsilsesquioxane nanocage used as the g factor standard are highlighted in yellow; three lines of the ⁵⁵Mn hyper-fine sextet, which are not superimposed with other signals, are highlighted in magenta. Mn²⁺ ions were present in the sample holder.

(high-field EPR). The signal at 9.7 GHz remained unresolved (Fig. S7, ESI†). However, the 9.7 GHz experiments at relatively low magnetic fields have a noteworthy advantage. At high magnetic fields, where the quantum numbers M_S correspond to the eigenfunctions of the spin Hamiltonian, EPR transitions $\Delta M_S \neq \pm 1$ are not allowed. However, at low fields, the eigenfunctions become linear combinations of the high-field states and quantum numbers M_S are not strictly applicable, thus the low intensity transitions $\Delta M_S \neq \pm 1$ (forbidden lines or half-field transitions) can be observed at ~ 1600 G⁴⁹. Even if a large modulation amplitude (10 G) was used, we did not observe the forbidden line for powder and frozen methanol solution of **1**. In systems with more than one semiquinone radical, the transitions $\Delta M_S \neq \pm 1$ are usually observed^{35–38,59,60} and thus the

lack of such a transition for **1** additionally confirms that it is a $S = \frac{1}{2}$ radical system.

The increase in frequency to 34 GHz revealed the g -anisotropy, but the signal was not completely resolved (Fig. S8, ESI†). However, a more complete resolution of the g tensor into its three components $g_z = 2.00204$, $g_y = 2.00377$, $g_x = 2.00455$ was obtained with the use of 406 GHz frequency (Fig. 5A), confirming high-field EPR as a unique technique for measuring g tensors of organic radicals with a good precision^{40,42,61–70}. Moreover, the line pattern of the spectra recorded at 406 GHz is consistent with a $S = \frac{1}{2}$ radical system, as there is no indication of any zero-field splitting^{67,71–75}.

The g_x and g_y principal components for **1** are significantly lower than the values we determined for the uncomplexed o-semiquinone radical of catechol ($g_z = 2.00233$, $g_y = 2.00534$, $g_x = 2.00573$; the spectrum is shown in Fig. 5B). The magnitude of this decrease is noticeably smaller in comparison with our observations for semiquinonato complexes of heavy cations (Hg^{2+} , Pb^{2+})^{40–42}, but it corresponds well to our previous DFT predictions for the complexes of lighter cations, that is Mg^{2+} and Ca^{2+} ^{76,77}.

This decrease in the g_y and g_x reflects changes in the molecular and electronic structure of the radical induced by the aluminium complexation. The values of g depend on the spin-orbit coupling and thus they differ significantly from $g_e = 2.002319$ (g parameter for the free electron) if the spin density is concentrated on heavier atoms⁷⁸. For organic radicals containing only light atoms the spin-orbit coupling is weak, but it is stronger for oxygen than for carbon atoms⁵⁰. Therefore, the reduction of g_y and g_x can be interpreted as the shift of spin density from the oxygen atoms towards the carbon atoms of the aromatic ring accompanied by the elongation of the C–O bonds in the o-semiquinone^{76,77,79}.

To confirm this conclusion and to propose a structure for **1** theoretical calculations were conducted using the ORCA program system^{80,81}. Molecular models ($S = \frac{1}{2}$) containing two

aluminium cations varying in coordination number (c.n. = 4, 5 or 6), one o-semiquinone radical anion (sq) and one catecholate (ct) ligand were used. The coordination sphere of Al^{3+} was completed with ligands available in the reaction mixture (H_2O and Cl^-) and OH^- (from possible hydrolysis of aluminium ions). The models were prepared using the structures determined by X-ray crystallography for comparable diamagnetic ($S = 0$) aluminium dimers^{44,45,82} and their structures were optimised at the UBP86/def2-TZVP level. In total 15 model complexes (**m1** – **m15**) were investigated computationally: $[\text{Al}_2(\text{sq})(\text{ct})(\text{Cl})_2]^+$ (**m1**, c.n. = 4), $[\text{Al}_2(\text{sq})(\text{ct})(\text{H}_2\text{O})_2]^{3+}$ (**m2**, c.n. = 4), $[\text{Al}_2(\text{sq})(\text{ct})(\text{OH})_2]^+$ (**m3**, c.n. = 4), $[\text{Al}_2(\text{sq})(\text{ct})(\text{Cl})_4]^-$ (**m4**, c.n. = 5), $[\text{Al}_2(\text{sq})(\text{ct})(\text{H}_2\text{O})_4]^{3+}$ (**m5**, c.n. = 5), $[\text{Al}_2(\text{sq})(\text{ct})(\text{OH})_4]^-$ (**m6**, c.n. = 5), $[\text{Al}_2(\text{sq})(\text{ct})(\text{Cl})_6]^{3-}$ (**m7**, **m10** and **m13**, c.n. = 6), $[\text{Al}_2(\text{sq})(\text{ct})(\text{H}_2\text{O})_6]^{3+}$ (**m8**, **m11** and **m14**, c.n. = 6), $[\text{Al}_2(\text{sq})(\text{ct})(\text{OH})_6]^{3-}$ (**m9**, **m12** and **m15**, c.n. = 6). The molecular structures, singly-occupied molecular orbital (SOMO) and spin density isosurfaces for models with H_2O molecules completing the coordination sphere of Al^{3+} (**m2**, **m5**, **m8**, **m11**, **m14**) are shown in Fig. 6 and in Fig. S9, ESI†, for the remaining models. Agreement between the experimental and theoretical EPR parameters was supposed to show which of the molecular models emulate the molecular and electronic structure of complex **1**. This approach was proven effective^{40–42,64,70,83–90}. The computations were also done for the uncomplexed radical (**r1**) and the radical with hydrogen bonded water (**r2**), EtOH (**r3**) and MeOH (**r4**) molecules (Fig. S10, ESI†).

Three functionals were used to compute the g tensors (B3LYP, PBE0 and TPSS0) in concert with the IGLO-II and IGLO-III basis sets. The results were not strongly dependent on the functional and basis set, as expected for semiquinonato complex of diamagnetic cation^{76,77}, and henceforth the results of the TPSS0/IGLO-III calculations are given in the text because this method was the most accurate in prediction of the g tensor components for the uncomplexed o-semiquinone (Table S1, ESI†).

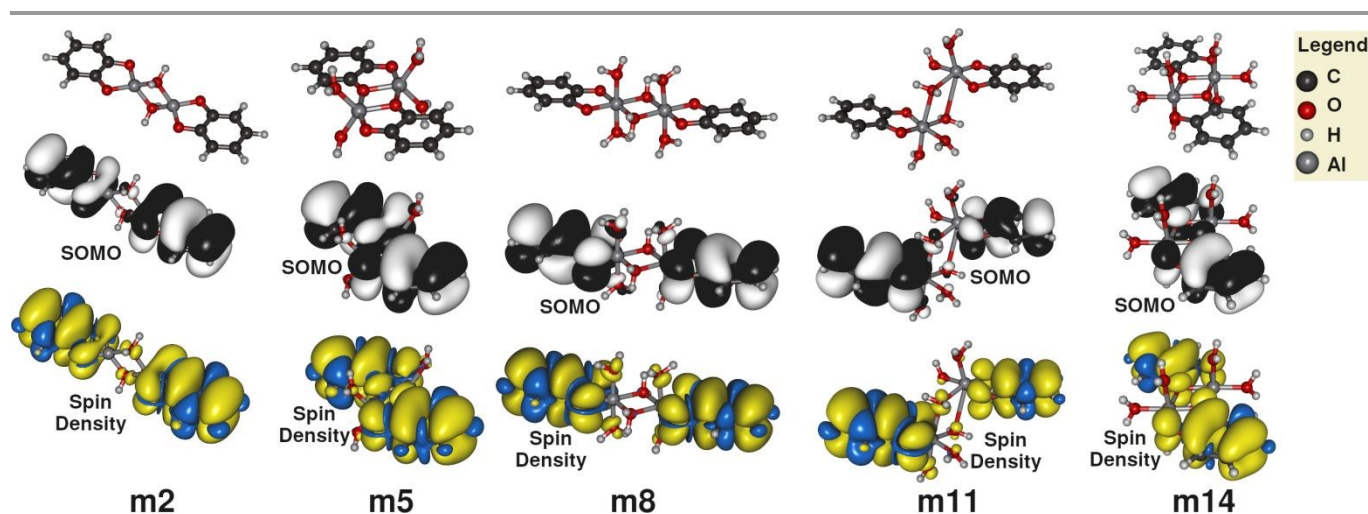


Fig. 6 Molecular models of the Al radical complex (**1**) with H_2O molecules completing the coordination sphere. The structure were optimized at the BP86/def2-TZVP level; the singly-occupied molecular orbitals (contoured at isovalue 10^{-2}) and spin densities (contoured at isovalue 10^{-4}) calculated at the B3LYP/IGLO-III level. The remaining models are shown in Fig S8, ESI†.

Table 2 The principal components of the \mathbf{g} tensor calculated at the TPSS0/IGLO-III level and the isotropic hyperfine coupling constant due to ^{27}Al (a_{Al}) calculated at the DLPNO-CCSD/IGLO-II level. The a_{Al} values are given in MHz. The results of other methods are given in Table S1 and S4, ESI†. DOI: 10.1039/D1CP01596F

model	c.n.	composition	TPSS0/IGLO-III				DLPNO-CCSD/IGLO-II
			g_z	g_y	g_x	g_{iso}	a_{Al}
m1	4	$[\text{Al}_2(\text{sq})(\text{ct})(\text{Cl})_2]^{+}$	2.00121	2.00458	2.00480	2.00353	-9.27
m2	4	$[\text{Al}_2(\text{sq})(\text{ct})(\text{H}_2\text{O})_2]^{+3+}$	2.00230	2.00387	2.00424	2.00347	-4.49
m3	4	$[\text{Al}_2(\text{sq})(\text{ct})(\text{OH})_2]^{+}$	2.00211	2.00469	2.00471	2.00384	-0.22
m4	5	$[\text{Al}_2(\text{sq})(\text{ct})(\text{Cl})_4]^{-}$	2.00423	2.00461	2.00516	2.00466	-6.66
m5	5	$[\text{Al}_2(\text{sq})(\text{ct})(\text{H}_2\text{O})_4]^{+3+}$	2.00238	2.00408	2.00453	2.00366	-3.21
m6	5	$[\text{Al}_2(\text{sq})(\text{ct})(\text{OH})_4]^{-}$	2.00235	2.00477	2.00537	2.00416	-7.07
m7	6	$[\text{Al}_2(\text{sq})(\text{ct})(\text{Cl})_6]^{3-}$	2.00076	2.00505	2.00770	2.00451	-11.14
m8	6	$[\text{Al}_2(\text{sq})(\text{ct})(\text{H}_2\text{O})_6]^{+3+}$	2.00233	2.00494	2.00574	2.00434	-6.56
m9	6	$[\text{Al}_2(\text{sq})(\text{ct})(\text{OH})_6]^{3-}$	2.00152	2.00591	2.00674	2.00472	-7.50
m10	6	$[\text{Al}_2(\text{sq})(\text{ct})(\text{Cl})_6]^{3-}$	2.00178	2.00528	2.00614	2.00440	-6.44
m11	6	$[\text{Al}_2(\text{sq})(\text{ct})(\text{H}_2\text{O})_6]^{3+}$	2.00231	2.00466	2.00474	2.00390	-4.99
m12	6	$[\text{Al}_2(\text{sq})(\text{ct})(\text{OH})_6]^{3-}$	2.00223	2.00533	2.00635	2.00464	-4.80
m13	6	$[\text{Al}_2(\text{sq})(\text{ct})(\text{Cl})_6]^{3-}$	2.00222	2.00589	2.00762	2.00524	-7.15
m14	6	$[\text{Al}_2(\text{sq})(\text{ct})(\text{H}_2\text{O})_6]^{+3+}$	2.00236	2.00450	2.00494	2.00393	-6.60
m15	6	$[\text{Al}_2(\text{sq})(\text{ct})(\text{OH})_6]^{3-}$	2.00225	2.00548	2.00643	2.00472	-5.39
		<i>experimental for complex 1</i>	<i>2.00204</i>	<i>2.00377</i>	<i>2.00455</i>	<i>2.00367</i>	<i>±2.5</i>
r1	–	sq^{-}	2.00218	2.00601	2.00667	2.00495	–
r2	–	$\text{sq}^{-} \times 3\text{H}_2\text{O}$	2.00219	2.00563	2.00608	2.00463	–
r3	–	$\text{sq}^{-} \times 3\text{EtOH}$	2.00222	2.00567	2.00619	2.00469	–
r4	–	$\text{sq}^{-} \times 3\text{MeOH}$	2.00222	2.00567	2.00618	2.00469	–
		<i>experimental for uncomplexed radical</i>	<i>2.00233</i>	<i>2.00534</i>	<i>2.00573</i>	<i>2.00469</i>	–

Regardless of the c.n. and additional ligands completing the aluminium coordination sphere, the DFT computations revealed that the spin density is uniformly distributed between the two organic ligands (Fig. 6 and S9, ESI†) without a significant concentration on the aluminium atoms. However, the additional ligands affect the spin density distribution and hence the computed \mathbf{g} tensors (Table 2 and S1, ESI†). Except for **m1**, in the case of models that include Cl^- (**m4**, **m7**, **m10** and **m13**) the \mathbf{g} tensor components were notably higher than the values we determined for **1**. For instance, the predicted g_z , g_y , and g_x values for **m4** are 2.00423, 2.00452 and 2.00534, respectively. The values of g_x and g_z for **m1** are close to the experimental counterparts, but g_y is considerably overestimated. Hence, all models with Cl^- coordinated to Al^{3+} seem not to be a proper representation of **1**. The high values of the \mathbf{g} tensor components predicted for these models can be explained by the noticeable spin population on the Cl atoms (Table S2, ESI†), which results in significant atomic contributions to the \mathbf{g} tensor from these atoms (Table S3, ESI†). These results reflect those of Demay-Drouhard et al. who found for perchlorotriphenylmethyl radical that the spin density on chlorine atoms has a strong effect on the \mathbf{g} tensor⁶¹.

For **m3**, which is a model with OH^- coordinated to Al^{3+} , DFT predicted too high g_y and g_x values and the insufficient difference between them (too axial \mathbf{g} tensor), namely $g_y = 2.00478$ and $g_x = 2.00493$. The overestimation of g_y and g_x is even more significant in the case of the remaining models with OH^- (**m6**, **m9**, **m12** and **m15**), which compellingly proves that these structures are not good theoretical models of the real Al^{3+} radical complex.

Among models with H_2O molecules completing the coordination sphere of Al^{3+} (**m2**, **m5**, **m8**, **m11**, **m14**), the agreement between the theoretically and experimentally obtained principal components of the \mathbf{g} tensor is generally satisfactory. For these models the calculated g_y and g_x values are slightly overestimated, but this should be expected for semiquinone radicals and their complexes with diamagnetic cations^{67,76,77,91,92}. Such overestimation of g_y and g_x is also observed in the DFT results for the uncomplexed radical (**r1**, **r2**, **r3** and **r4**). Nevertheless, the overestimation of g_y and g_x varies between models with H_2O and is noticeably larger for **m14**, **m11** and **m8** than for **m5** and **m2**.

Although the \mathbf{g} tensor for **m2** is mostly in line with the 406.4 GHz EPR experiment, **m2** seems an inaccurate model of **1**. Dialuminium complexes with water molecules playing the role

of bridging ligands are known⁹³, but they are unlikely to sustain their dimeric form in polar solvents. Hyperfine splitting observed in the liquid phase (methanol) EPR spectrum of **1** empirically proves that **1** comprises two Al³⁺ ions in the paramagnetic unit, hence **m5** with bridging anionic organic ligands appears as a more appropriate model.

Support for this conclusion can be provided by the theoretical prediction of the isotropic hyperfine interaction constant a_{Al} . It was performed with a vast array of exchange-correlation density functionals that were shown to yield sufficiently accurate hyperfine constants for the uncomplexed o-semiquinone radical and its Mg²⁺ complex⁹⁴, namely B3LYP, PBE0, TPSS0, ω B97X, B2PLYP, mPW2PLYP and DSD-BLYP. Moreover, the highly accurate domain based local pair natural orbital CCSD method (DLPNO-CCSD)^{95–97} was used as it was shown as highly reliable and generally superior to DFT in theoretical studies of isotropic hyperfine interaction^{94,97}. Henceforth the results of the DLPNO-CCSD/IGLO-II calculations are given in the text. The DLPNO-CCSD calculations with larger IGLO-III were prohibitively expensive.

The results of the DLPNO-CCSD calculations presented in Table 2 show that for all models with H₂O molecules completing the coordination sphere of Al³⁺ the absolute values of a_{Al} are overestimated: 4.49, 3.21, 6.56, 4.99 and 6.60 MHz for **m2**, **m5**, **m8**, **m11** and **m14**, respectively. Nevertheless, the absolute value of a_{Al} predicted for **m5** is close to its experimental counterpart, significantly closer than a_{Al} for **m2**. This comparison between **m2** and **m5** corroborates the conclusion that **m5** is a more accurate model of **1**. The predicted values of a_{Al} for models with OH⁻ and Cl⁻ in the Al³⁺ coordination sphere are not in accordance with the EPR results. Moreover, the hyperfine constants due to ¹H calculated for the model complexes are noticeably lower in comparison with their counterparts for the uncomplexed radical (Table S4, ESI[†]). For example, according to the DLPNO-CCSD calculations, they decrease in magnitude from -2.22 and -10.29 MHz for **r4** to -0.57 and -1.13 MHz, respectively, for **m5**. Such a low magnitude might hinder the experimental detection of these hyperfine interactions.

The theoretical calculations were also performed for the $S = 1$ counterparts of **m2**, **m5**, **m8**, **m11** and **m14**. Although the experimental components of the g tensor (Table S5, ESI[†]) were reasonably reproduced in these calculations, except for **m8**($S=1$) and **m11**($S=1$), the isotropic hyperfine coupling constants due to ²⁷Al and ¹H are not in line with our EPR experiments (Table S6 and S7, ESI[†]). The coupling constants due to ²⁷Al are larger and the magnitude of one of the ¹H constants is large enough for experimental detection. For example, the a_{Al} value for the $S = 1$ counterpart of **m5** was predicted at the DLPNO-CCSD level to be -6.75 MHz, while the coupling constants due to ¹H were -0.11 and -8.33 MHz. These results support the conclusion that **1** is not a $S = 1$ system.

Based on EPR parameters, we hypothesised that the reduction of g_y and g_x observed for **1** in comparison with the uncomplexed radical can be interpreted as the shift of spin density from the oxygen atoms towards the carbon atoms of the aromatic ring accompanied by the elongation of the C–O bonds

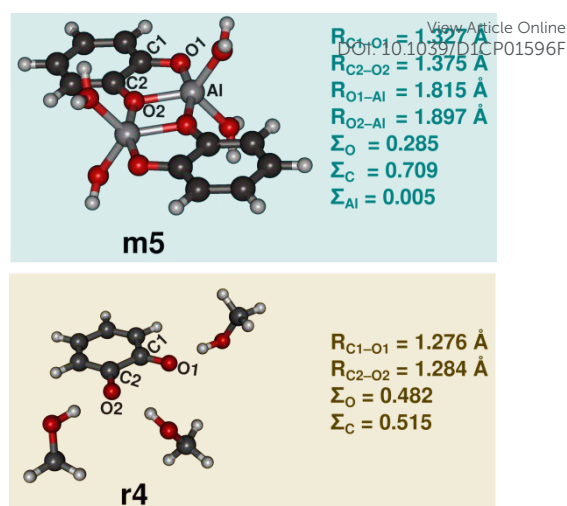


Fig. 6 Selected bond lengths (R) and total Löwdin spin populations for groups of atoms (Σ) for the model complex **m5** and uncomplexed o-semiquinone anion with three H-bonded MeOH molecules (**r4**).

in the o-semiquinone. The theoretical computations for **m5** confirm this assumption. In comparison with **r4** (o-semiquinone with three H-bonded MeOH molecules) the C–O bonds are lengthened from 1.276 and 1.284 Å to 1.327 Å and 1.375 Å, while the total spin population on the O atoms declines from 0.482 to 0.285 (Fig. 6).

Conclusions

In summary, we showed that o-semiquinone radical can be isolated as an amorphous mono-semiquinonato ($S = \frac{1}{2}$) aluminium complex in a short procedure. Using multifrequency EPR spectroscopy combined with computational DFT and DLPNO-CCSD techniques, we demonstrated that it is a species $\text{Al}_2(\text{C}_6\text{H}_4\text{O}_2)_2\text{Cl}_3(\text{H}_2\text{O})_6$, composed of two equivalent aluminium cations and two catechol-like ligands with the unpaired electron uniformly distributed between them.

The complex **1** can stay unchanged under ambient conditions for at least a few months. The model **m5** can be used to analyse factors determining its stability. In this model the redox-inactive Al³⁺ cations form six bonds with the hydroxyl oxygen atoms and thus efficiently restrict the access to the active spin sites. Much of the stability of **1** can be also attributed to the theoretically predicted delocalisation of the unpaired electron on two organic ligands. For the majority of mono-semiquinonato complexes of diamagnetic metals the EPR measurements and theoretical predictions at DFT level suggested that the unpaired electron is localised on one organic ligand^{40,41,76,77,98–100}. The persistent mono-semiquinonato complexes of Pb²⁺ that we reported previously support the important role of the unpaired electron delocalisation in stability of **1**. For that persistent $S = \frac{1}{2}$ radical complex of this heavy cation, similar delocalisation of the unpaired electron between two organic ligands was postulated⁴².

As discussed in ref. 101 and 102, porous radical systems can find future applications as systems for transition-metal-free

aerobic reactions and our ongoing efforts focus on structural modifications of **1** that will allow to check the effect of radical centres in nanopores on such reactions.

Experimental

Materials

All reagents were purchased from Sigma-Aldrich/Merck and used without further purification. 1,2-dihydroxybenzene (catechol or pyrocatechol), aluminium chloride hexahydrate, iodine and solvents (acetone, methanol, propan-2-ol and chloroform) were of at least 98% purity. Hydrogen peroxide was used as a water solution (30% wt., containing inhibitor).

Generating radical systems

To obtain the Al³⁺ complex containing o-semiquinonato ligand ground aluminium chloride hexahydrate (1 mmol, 240 mg) was added to a solution of catechol (1 mmol, 110 mg) in methanol (10 mL) under stirring. The resulting mixture was gently warmed for 30 minutes and then iodine (0.25 mmol, 64 mg) in methanol (5 mL) was added dropwise. The resultant dark blue solution was heated to 50 °C and stirred for 1.5 h. The volume of the mixture was reduced to a fourth and filtered. 10 mL of diethyl ether was added and the dark blue product (**1**) precipitated overnight. The product was washed off with cold diethyl ether and recrystallized from propan-2-ol (again diethyl ether was used to precipitate **1**). The radical complex was stable under ambient conditions.

To obtain the uncomplexed and unstable o-semiquinone radical of catechol, a drop of hydrogen peroxide solution was added to 1 mmol (110 mg) of catechol in 5 mL of methanol under stirring. The solution became brown and the EPR spectrum was recorded. The radical remained EPR-detectable for a few minutes. Using hydrogen peroxide was found more efficient than the ambient oxygen oxidation in the alkaline methanolic solution we used previously⁶⁷.

Physical measurements

The EPR spectra at 9.6 GHz (X-band) and 34 GHz (Q-band) frequencies were recorded using a Bruker Elexsys E500 spectrometer equipped with a NMR teslameter and a frequency counter. The high-field EPR spectra at a frequency of 406.4 GHz were recorded at the EMR facility of the NHMFL (<https://nationalmaglab.org/user-facilities/emr>) using a home-built spectrometer. The instrument is a transmission-type device, using no resonance cavity, in which waves are propagated in cylindrical lightpipes. The microwaves were generated by a phase-locked oscillator (Virginia Diodes) operating at a frequency of 8-20 GHz. That frequency was supplied to a chain of frequency multipliers generating the 2nd, 4th, 8th, 16th, 24th, 32nd and 48th harmonics. The frequency is accurate to better than 7 significant digits. A superconducting magnet (Oxford Instruments) capable of reaching a field of 17 T was employed. Modulation frequency of 50 kHz were used in concert with amplitudes of 5 and 10 G, but these values of amplitudes are approximate due to the instrument limitation.

Atomic hydrogen trapped in octaisobutylsilsesquioxane nanocage was used as the g factor standard for the high-field EPR measurements¹⁰³. In the quantitative EPR experiment irradiated alanine pill (Bruker, 1.7×10^{17} spins) were used.

The solution EPR spectra were recorded in methanol (20 mg of **1** in 1 mL). The powder EPR spectra were a program written by A.O. (<https://nationalmaglab.org/user-facilities/emr/emr-resources/spin-software>). The isotropic EPR spectra were simulated using the SimFonia program developed by Bruker.

The powder X-ray diffraction patterns (XRD) were measured by a D8 Advance Diffractometer from Bruker with Ni-filtered CuK α 1 radiation ($\lambda = 1.540596 \text{ \AA}$) in the range of $2\theta = 15\text{--}70^\circ$, and with the step of $2\theta = 0.008^\circ$.

The morphology of the radical complex was observed by scanning electron microscopy (SEM) using a Hitachi S-3400N equipped with an energy dispersive X-ray (EDX) spectroscopy EDAX analyser.

Differential scanning calorimetry (DSC) was used to investigate the melting behaviour. These experiments were carried out with the use of a Mettler-Toledo DSC 3 calorimeter. Aluminium pans were loaded and hermetically sealed; empty pans used as the reference. Samples were submitted to two heating and two cooling runs from -160 °C to 115 °C and a rate of 10 K/min was used. Thermogravimetric analyses (TG-DTA) were carried out using a Setaram SETSYS 16/18 thermogravimetric analyser, operated under nitrogen atmosphere, with a heating rate of 10 K/min between 40 and 1000 °C (sample mass about 10 mg). The results were expressed in terms of percent weight loss with respect to temperature.

Measurements of conventional gas adsorption isotherms were conducted using a Micromeritics ASAP 2020 HD volumetric instrument under continuous adsorption conditions. Brunauer–Emmet–Teller (BET) analyses were carried out to determine the total specific surface areas for the N₂ isotherms at 77 K.

The elemental analyses were carried out on a CHNS Vario EL Cube (Elementar) elemental analyser.

Magnetic measurements were conducted using a Quantum Design SQUID-based MPMSXL-5 magnetometer equipped with a superconducting magnet. The magnetometer was calibrated with the palladium rod sample (Materials Research Corporation, measured purity 99.9985%). The magnetic susceptibility data of a powder sample were measured over the temperature range 1.8–300 K at a magnetic induction of 5000 G. The corrections for the sample holder and diamagnetism of the constituent atoms, the last calculated from the Pascal constants¹⁰⁴, were taken into account.

Theoretical calculations

All the calculations were performed with the ORCA 4.1.1/4.2.1 suite of programs^{80,81}. Molecular structures were optimised at the DFT level using the gradient-corrected BP86 functional^{105,106} of Becke and Perdew combined with the def2-TZVP basis set developed by Ahlrichs and co-workers^{107,108}. As the resolution of the identity approximation in the Split-RI¹⁰⁹ variant was used, an appropriate auxiliary basis set (def2/J) was

employed¹¹⁰. The conductor-like polarizable continuum model (CPCM)¹¹¹ was used to cover the solvent effects. This approach was showed to provide accurate molecular structures for open-shell systems^{112,113}. Each of the stationary points was fully characterised as a true minimum through a vibrational analysis.

The **g** matrices (**g** tensors) were computed using Neese's coupled perturbed Kohn–Sham (CPKS) method¹¹⁴ and an accurate spin-orbit coupling operator [RI-SOMF(1X)]¹¹⁵. The CPCM method was used again to cover the solvent effects. For these computations, the hybrid generalised gradient approximations B3LYP^{116–118} and PBE0^{119,120} as well as the hybrid meta-generalised gradient approximation TPSS0^{121–123} (a version of TPSSh¹²³ with 25% of the HF exchange). The functionals B3LYP and PBE0 were successfully used in the computational approach to the **g** tensor of, inter alia, nitroxide^{124–126} and semiquinone radicals^{76,77,79,92,127–129}. The functional TPSS0 was highly efficient at the computational reproduction of hyperfine coupling constants for o-semiquinone and its Mg²⁺ complex⁹⁴, hence expected to yield accurate electronic structures and other properties for such systems.

The isotropic hyperfine coupling constant due to ²⁷Al (*a*_{Al}) was calculated as described in the literature^{130–132} using a vast array of DFT methods, namely the hybrid generalised gradient approximations B3LYP^{116–118} and PBE0^{119,120}; the hybrid meta-generalized gradient approximation TPSS0^{121–123}; the range-separated hybrid generalised gradient approximation ωB97X¹³³; and the double hybrid generalised gradient approximations B2PLYP¹³⁴, mPW2PLYP¹³⁵ and DSD-BLYP¹³⁶. These functionals were selected because they performed well in a recent benchmark study that included o-semiquinone radical and its Mg²⁺ complex⁹⁴. In addition, the *a*_{Al} values were predicted by the domain-based local pair-natural orbital coupled-cluster with singles and doubles (DLPNO-CCSD) method^{97,137–139}, which was designed to make the CC theory broadly applicable. This technique has been showed to be highly accurate in the hyperfine coupling constant calculations^{94,97} and was used here with the truncation settings recommended for this purpose⁹⁷. The open-shell DLPNO-CCSD calculations were carried out using the reference determinants build from quasi-restricted orbitals (QROs) from the unrestricted Hartree-Fock (UHF) calculations. QROs should closely resemble the restricted open-shell Hartree-Fock (ROHF) orbitals¹⁴⁰. The validity of the DLPNO-CCSD results was assessed using the T1 diagnostic parameter. The observed values of T1 were always noticeably lower than 0.02.

The **g** matrix is a valence and semi-core property, and therefore relatively insensitive to the choice of the basis set. For organic radicals, even modest split-valence basis sets with one polarisation function in the valence region bring about reasonable results. If a polarised triple- ζ basis set is used, results become close to saturation^{67,79,92,124,141}. However, the calculations of hyperfine coupling constants are widely known for having strict basis set requirements, especially in the core region^{130–132,142}. Therefore, the IGLO-II and IGLO-III basis sets were employed in this work for both the *a*_{Al} and **g** tensor calculations¹⁴³. For the *a*_{Al} and **g** tensor calculations, the

auxiliary basis sets were generated using the AutoAux¹⁴⁴ procedure available in ORCA. DOI: 10.1039/D1CP01596F

Conflicts of interest

There are no conflicts to declare.

Acknowledgements

We dedicate this paper to Professor Adam Jezierski on the occasion of his honourable retirement. This work was financially supported by the National Science Centre, Poland (Narodowe Centrum Nauki, nr rej. 2018/02/X/ST5/01186). All computations were performed using computers of the Wroclaw Center for Networking and Supercomputing (Grant No. 47). A portion of this work was performed at the National High Magnetic Field Laboratory, which is supported by NSF Cooperative Agreement DMR-1644779 and the State of Florida.

References

- 1 M. Gomberg, *J. Am. Chem. Soc.*, 1900, **22**, 757–771.
- 2 S. Crespi and M. Fagnoni, *Chem. Rev.*, 2020, **120**, 9790–9833.
- 3 N. Kvasovs and V. Gevorgyan, *Chem. Soc. Rev.*, 2021, **50**, 2244–2259.
- 4 C. Fleming, D. Chung, S. Ponce, D. J. R. Brook, J. Daros, R. Das, A. Ozarowski and S. A. Stoian, *Chem. Commun.*, 2020, **56**, 4400–4403.
- 5 M. Epshtein, V. Scutelnic, Z. Yang, T. Xue, M. L. Vidal, A. I. Krylov, S. Coriani and S. R. Leone, *J. Phys. Chem. A*, 2020, **124**, 9524–9531.
- 6 M. L. Vidal, M. Epshtein, V. Scutelnic, Z. Yang, T. Xue, S. R. Leone, A. I. Krylov and S. Coriani, *J. Phys. Chem. A*, 2020, **124**, 9532–9541.
- 7 F. Dénès, M. Pichowicz, G. Povie and P. Renaud, *Chem. Rev.*, 2014, **114**, 2587–2693.
- 8 R. Akisaka, Y. Ohga and M. Abe, *Phys. Chem. Chem. Phys.*, 2020, **22**, 27949–27954.
- 9 H. Cui, D. Xiao, L. Zhang, H. Ruan, Y. Fang, Y. Zhao, G. Tan, L. Zhao, G. Frenking, M. Driess and X. Wang, *Chem. Commun.*, 2020, **56**, 2167–2170.
- 10 K. M. Nakafuku, S. C. Fosu and D. A. Nagib, *J. Am. Chem. Soc.*, 2018, **140**, 11202–11205.
- 11 S. So, B. B. Kirk, U. Wille, A. J. Trevitt, S. J. Blanksby and G. da Silva, *Phys. Chem. Chem. Phys.*, 2020, **22**, 2130–2141.
- 12 L. Vereecken, P. T. M. Carlsson, A. Novelli, F. Bernard, S. S. Brown, C. Cho, J. N. Crowley, H. Fuchs, W. Mellouki, D. Reimer, J. Shenolikar, R. Tillmann, L. Zhou, A. Kiendler-Scharr and A. Wahner, *Phys. Chem. Chem. Phys.*, 2021, **23**, 5496–5515.
- 13 S. Sarkar, K. P. S. Cheung and V. Gevorgyan, *Chem. Sci.*, 2020, **11**, 12974–12993.
- 14 J. Shukla, S. Kumar, Rustam and P. Mukhopadhyay, *Org. Lett.*, 2020, **22**, 6229–6233.
- 15 R. G. Hicks, Ed., *Stable Radicals*, John Wiley & Sons, Ltd,

- Chichester, UK, 2010.
- 16 I. Ratera and J. Veciana, *Chem. Soc. Rev.*, 2012, **41**, 303–349.
- 17 K. E. Vostrikova, *Coord. Chem. Rev.*, 2008, **252**, 1409–1419.
- 18 S. Demir, I. R. Jeon, J. R. Long and T. D. Harris, *Coord. Chem. Rev.*, 2015, **289–290**, 149–176.
- 19 K. Chakarawet, T. D. Harris and J. R. Long, *Chem. Sci.*, 2020, **11**, 8196–8203.
- 20 Y. Imada, H. Nakano, K. Furukawa, R. Kishi, M. Nakano, H. Maruyama, M. Nakamoto, A. Sekiguchi, M. Ogawa, T. Ohta and Y. Yamamoto, *J. Am. Chem. Soc.*, 2016, **138**, 479–482.
- 21 X. Ai, E. W. Evans, S. Dong, A. J. Gillett, H. Guo, Y. Chen, T. J. H. Hele, R. H. Friend and F. Li, *Nature*, 2018, **563**, 536–540.
- 22 C. He, Z. Li, Y. Lei, W. Zou and B. Suo, *J. Phys. Chem. Lett.*, 2019, **10**, 574–580.
- 23 J. Zeng, S. Bin Qiu, Y. J. Zhao, X. B. Yang and Y. Yao, *J. Phys. Chem. Lett.*, 2020, **11**, 1194–1198.
- 24 J. Exner, I. Maisuls, A. Massolle, S. Klabunde, M. R. Hansen, C. A. Strassert, J. Neugebauer, H. Eckert and A. Studer, *Phys. Chem. Chem. Phys.*, 2021, **23**, 2999–3007.
- 25 G. Moise, L. Tejerina, M. Rickhaus, H. L. Anderson and C. R. Timmel, *J. Phys. Chem. Lett.*, 2019, **10**, 5708–5712.
- 26 A. A. Hande, C. Darrigan, P. Bartos, P. Baylère, A. Pietrzak, P. Kaszyński and A. Chrostowska, *Phys. Chem. Chem. Phys.*, 2020, **22**, 23637–23644.
- 27 T. Sugawara, H. Komatsu and K. Suzuki, *Chem. Soc. Rev.*, 2011, **40**, 3105–3118.
- 28 B. Tang, J. Zhao, J.-F. Xu and X. Zhang, *Chem. Sci.*, 2020, **11**, 1192–1204.
- 29 A. A. Zolotukhin, M. P. Bubnov, A. V. Arapova, G. K. Fukin, R. V. Romyantsev, A. S. Bogomyakov, A. V. Knyazev and V. K. Cherkasov, *Inorg. Chem.*, 2017, **56**, 14751–14754.
- 30 M. P. Bubnov, N. A. Skorodumova, A. V. Arapova, N. N. Smirnova, M. A. Samsonov, G. K. Fukin, V. K. Cherkasov and G. A. Abakumov, *Inorg. Chem.*, 2015, **54**, 7767–7773.
- 31 P. A. Abramov, N. P. Gritsan, E. A. Suturina, A. S. Bogomyakov and M. N. Sokolov, *Inorg. Chem.*, 2015, **54**, 6727–6735.
- 32 P. Verma, J. Weir, L. Mirica and T. D. P. Stack, *Inorg. Chem.*, 2011, **50**, 9816–9825.
- 33 I. Casanova, A. Sousa-Pedrares, J. Viqueira, M. L. Durán, J. Romero, A. Sousa and J. A. García-Vázquez, *New J. Chem.*, 2013, **37**, 2303–2316.
- 34 P. Sarkar, A. Sarmah and C. Mukherjee, *Chem. Commun.*, 2021, **57**, 1352–1355.
- 35 A. Ozarowski, B. R. McGarvey, A. El-Hadad, Z. Tian, D. G. Tuck, D. J. Krovich and G. C. DeFotis, *Inorg. Chem.*, 1993, **32**, 841–847.
- 36 A. Ozarowski, B. R. McGarvey, C. Peppe and D. G. Tuck, *J. Am. Chem. Soc.*, 1991, **113**, 3288–3293.
- 37 A. V. Piskunov, I. N. Meshcheryakova, A. V. Maleeva, A. S. Bogomyakov, G. K. Fukin, V. K. Cherkasov and G. A. Abakumov, *Eur. J. Inorg. Chem.*, 2014, **2014**, 3252–3258.
- 38 C. W. Lange, B. J. Conklin and C. G. Pierpont, *Inorg. Chem.*, 1994, **33**, 1276–1283.
- 39 C. Das, P. Shukla, L. Sorace and M. Shanmugam, *Dalt. Trans.*, 2017, **46**, 1439–1448.
- 40 M. Witwicki, M. Jerzykiewicz and A. Ozarowski, *New Article Online Chemosphere*, 2015, **119**, 479–484. DOI: 10.1039/D1CP01596F
- 41 M. Jerzykiewicz, M. Witwicki and J. Jezierska, *Chemosphere*, 2015, **138**, 233–238.
- 42 M. Witwicki, M. Jerzykiewicz, A. R. Jaszewski, J. Jezierska and A. Ozarowski, *J. Phys. Chem. A*, 2009, **113**, 14115–14122.
- 43 T. A. Annan, D. H. McConville, B. R. McGarvey, A. Ozarowski and D. G. Tuck, *Inorg. Chem.*, 1989, **28**, 1644–1648.
- 44 M. H. Chisholm, J. Gallucci, D. Navarro-Llobet and H. Zhen, *Polyhedron*, 2003, **22**, 557–561.
- 45 D. G. Hendershot, M. Barber, R. Kumar and J. P. Oliver, *Organometallics*, 1991, **10**, 3302–3309.
- 46 D. R. Eaton, *Inorg. Chem.*, 1964, **3**, 1268–1271.
- 47 S. Dedroog, T. Pas, B. Vergauwen, C. Huygens and G. Van den Mooter, *J. Pharm. Biomed. Anal.*, 2020, **178**, 112937.
- 48 P. Sharma, J. Yeo, D. K. Kim and C. H. Cho, *J. Mater. Chem.*, 2012, **22**, 2838.
- 49 J. Weil and J. Bolton, *Electron Paramagnetic Resonance: Elementary Theory and Practical Applications*, John Wiley & Sons, Inc., Hoboken, Second Edi., 2006.
- 50 F. Gerson and W. Huber, *Electron Spin Resonance Spectroscopy of Organic Radicals*, Wiley-VCH, Weinheim, First., 2003.
- 51 C. J. O'Connor, in *Progress in Inorganic Chemistry*, ed. S. J. Lippard, John Wiley & Sons, Inc., New York, 1982, vol. 29, pp. 203–283.
- 52 G. V. R. Chandramouli, C. Balagopalakrishna, M. V. Rajasekharan and P. T. Manoharan, *Comput. Chem.*, 1996, **20**, 353–358.
- 53 C. P. Constantinides, P. A. Koutentis, H. Krassos, J. M. Rawson and A. J. Tasiopoulos, *J. Org. Chem.*, 2011, **76**, 2798–2806.
- 54 C. P. Constantinides, P. A. Koutentis, H. Krassos, J. M. Rawson and A. J. Tasiopoulos, *J. Org. Chem.*, 2011, **76**, 2798–2806.
- 55 B. Cage, J. H. McNeely, S. E. Russek and H. J. Halpern, *J. Appl. Phys.*, , DOI:10.1063/1.3073992.
- 56 G. R. Eaton, S. S. Eaton, D. P. Barr and R. T. Weber, *Quantitative EPR*, Springer Vienna, Vienna, 2010.
- 57 L. B. Knight and W. Weltner, *J. Chem. Phys.*, 1971, **55**, 5066–5077.
- 58 M. Witwicki, *Int. J. Quantum Chem.*, 2018, **118**, e25779.
- 59 D. A. Shultz, A. K. Boal and G. T. Farmer, *J. Org. Chem.*, 1998, **63**, 9462–9469.
- 60 T. A. Annan, B. R. McGarvey, A. Ozarowski, D. G. Tuck and R. K. Chadha, *J. Chem. Soc., Dalt. Trans.*, 1989, 439–446.
- 61 P. Demay-Drouhard, H. Y. V. Ching, C. Decroos, R. Guillot, Y. Li, L. C. Tabares, C. Policar, H. C. Bertrand and S. Un, *Phys. Chem. Chem. Phys.*, 2020, **22**, 20792–20800.
- 62 J. Soetbeer, P. Gast, J. J. Walsh, Y. Zhao, C. George, C. Yang, T. M. Swager, R. G. Griffin and G. Mathies, *Phys. Chem. Chem. Phys.*, 2018, **20**, 25506–25517.
- 63 M. Malferrari, A. Savitsky, W. Lubitz, K. Möbius and G. Venturoli, *J. Phys. Chem. Lett.*, 2016, **7**, 4871–4877.
- 64 J. Niklas, K. L. Mardis and O. G. Poluektov, *J. Phys. Chem.*

- Let., 2018, **9**, 3915–3921.
- 65 A. Nalepa, K. Möbius, M. Plato, W. Lubitz and A. Savitsky, *Appl. Magn. Reson.*, 2019, **50**, 1–16.
- 66 S. Stoll, in *Electron Paramagnetic Resonance: Volume 22*, The Royal Society of Chemistry, 2011, pp. 107–154.
- 67 M. Witwicki, J. Jezierska and A. Ozarowski, *Chem. Phys. Lett.*, 2009, **473**, 160–166.
- 68 K. C. Christoforidis, S. Un and Y. Deligiannakis, *Environ. Sci. Technol.*, 2010, **44**, 7011–7016.
- 69 K. C. Christoforidis, S. Un and Y. Deligiannakis, *J. Phys. Chem. A*, 2007, **111**, 11860–11866.
- 70 I. Davis, T. Koto, J. R. Terrell, A. Kozhanov, J. Krzystek and A. Liu, *J. Phys. Chem. A*, 2018, **122**, 3170–3176.
- 71 R. Calvo, R. A. Isaacson, M. L. Paddock, E. C. Abresch, M. Y. Okamura, A. Maniero, L. Brunel and G. Feher, *J. Phys. Chem. B*, 2001, **105**, 4053–4057.
- 72 R. Calvo, E. C. Abresch, R. Bittl, G. Feher, W. Hofbauer, R. A. Isaacson, W. Lubitz, M. Y. Okamura and M. L. Paddock, *J. Am. Chem. Soc.*, 2000, **122**, 7327–7341.
- 73 Y. S. Lebedev, *Appl. Magn. Reson.*, 1994, **7**, 339–362.
- 74 S. Stoll, A. Gunn, M. Brynda, W. Sughrue, A. C. Kohler, A. Ozarowski, A. J. Fisher, J. C. Lagarias and R. D. Britt, *J. Am. Chem. Soc.*, 2009, **131**, 1986–1995.
- 75 S. Stoll, H. S. Shafaat, J. Krzystek, A. Ozarowski, M. J. Tauber, J. E. Kim and R. D. Britt, *J. Am. Chem. Soc.*, 2011, **133**, 18098–18101.
- 76 M. Witwicki and J. Jezierska, *J. Phys. Chem. B*, 2011, **115**, 3172–3184.
- 77 M. Witwicki and J. Jezierska, *Theor. Chem. Acc.*, 2013, **132**, 1383.
- 78 G. E. Cutsail, *Dalt. Trans.*, 2020, **49**, 12128–12135.
- 79 I. Ciofini, R. Reviakine, A. Arbuzyanov and M. Kaupp, *Theor. Chem. Acc.*, 2004, **111**, 132–140.
- 80 F. Neese, *Wiley Interdiscip. Rev. Comput. Mol. Sci.*, 2018, **8**, e1327.
- 81 F. Neese, F. Wennmohs, U. Becker and C. Riplinger, *J. Chem. Phys.*, 2020, **152**, 224108.
- 82 W. Ziemkowska, P. Zuk, M. K. Cyrański and A. Kunicki, *J. Mol. Struct.*, 2011, **1006**, 606–610.
- 83 R. Šolc, M. H. Gerzabek, H. Lischka and D. Tunega, *Comput. Theor. Chem.*, 2014, **1032**, 42–49.
- 84 N. Babaei Bidmeshki, Y. T. Azar, F. Ziaie and M. Janbazi, *Phys. Chem. Chem. Phys.*, 2021, 6815–6822.
- 85 M. Witwicki and J. Jezierska, *Geochim. Cosmochim. Acta*, 2012, **86**, 384–391.
- 86 A. T. Taguchi, P. J. O'Malley, C. A. Wraight and S. A. Dikanov, *J. Phys. Chem. B*, 2017, **121**, 10256–10268.
- 87 C. Sun, A. T. Taguchi, J. V. Vermaas, N. J. Beal, P. J. O'Malley, E. Tajkhorshid, R. B. Gennis and S. A. Dikanov, *Biochemistry*, 2016, **55**, 5714–5725.
- 88 S. Dasgupta, J. Adhikary, S. Giri, A. Bauza, A. Frontera and D. Das, *Dalt. Trans.*, 2017, **46**, 5888–5900.
- 89 O. G. Poluektov, J. Niklas and L. M. Utschig, *J. Phys. Chem. B*, 2019, **123**, 7536–7544.
- 90 K. F. Pirker, C. W. M. Kay, K. Stolze, D. Tunega, T. G. Reichenauer and B. A. Goodman, *Free Radic. Res.*, 2009, **43**, 47–57.
- 91 S. Sinnecker, E. Reijerse, F. Neese and W. Lubitz, *J. Am. Chem. Soc.*, 2004, **126**, 3280–3290. DOI: 10.1039/D1CP01596F
- 92 M. Kaupp, C. Remenyi, J. Vaara, O. L. Malkina and V. G. Malkin, *J. Am. Chem. Soc.*, 2002, **124**, 2709–2722.
- 93 Y. Chen, T. Wei, Z. Zhang, T. Chen, J. Li, J. Qiang, J. Lv, F. Wang and X. Chen, *Ind. Eng. Chem. Res.*, 2017, **56**, 12267–12275.
- 94 M. Witwicki, P. K. P. K. Walencik and J. Jezierska, *J. Mol. Model.*, 2020, **26**, 10.
- 95 M. Saitow, U. Becker, C. Riplinger, E. F. Valeev and F. Neese, *J. Chem. Phys.*, 2017, **146**, 164105.
- 96 D. Datta, S. Kossmann and F. Neese, *J. Chem. Phys.*, 2016, **145**, 114101.
- 97 M. Saitow and F. Neese, *J. Chem. Phys.*, 2018, **149**, 034104.
- 98 A. V. Lebedev, M. V. Ivanova, A. A. Timoshin and E. K. Ruuge, *ChemPhysChem*, 2007, **8**, 1863–1869.
- 99 J. Yuasa, T. Suenobu and S. Fukuzumi, *ChemPhysChem*, 2006, **7**, 942–954.
- 100 S. Fukuzumi, K. Ohkubo and Y. Morimoto, *Phys. Chem. Chem. Phys.*, 2012, **14**, 8472–8484.
- 101 Y. X. Tan, Y. P. He, D. Yuan and J. Zhang, *Appl. Catal. B Environ.*, 2018, **221**, 664–669.
- 102 G. Chen, Y. Zhang, K. Liu, X. Liu, L. Wu, H. Zhong, X. Dang, M. Tong and Z. Long, *J. Mater. Chem. A*, 2021, **9**, 7556–7565.
- 103 S. Stoll, A. Ozarowski, R. D. Britt and A. Angerhofer, *J. Magn. Reson.*, 2010, **207**, 158–163.
- 104 G. A. Bain and J. F. Berry, *J. Chem. Educ.*, 2008, **85**, 532–536.
- 105 A. D. Becke, *Phys. Rev. A*, 1988, **38**, 3098–3100.
- 106 J. P. Perdew, *Phys. Rev. B*, 1986, **33**, 8822–8824.
- 107 F. Weigend and R. Ahlrichs, *Phys. Chem. Chem. Phys.*, 2005, **7**, 3297.
- 108 A. Schäfer, H. Horn and R. Ahlrichs, *J. Chem. Phys.*, 1992, **97**, 2571–2577.
- 109 F. Neese, *J. Comput. Chem.*, 2003, **24**, 1740–1747.
- 110 F. Weigend, *Phys. Chem. Chem. Phys.*, 2006, **8**, 1057.
- 111 V. Barone and M. Cossi, *J. Phys. Chem. A*, 1998, **102**, 1995–2001.
- 112 F. Neese, W. Ames, G. Christian, M. Kampa, D. G. Liakos, D. A. Pantazis, M. Roemelt, P. Surawatanawong and Y. E. Shengfa, 2010, pp. 301–349.
- 113 M. Witwicki, *ChemPhysChem*, 2015, **16**, 1912–1925.
- 114 F. Neese, *J. Chem. Phys.*, 2001, **115**, 11080–11096.
- 115 F. Neese, *J. Chem. Phys.*, 2005, **122**, 034107.
- 116 A. D. Becke, *J. Chem. Phys.*, 1993, **98**, 5648–5652.
- 117 C. Lee, W. Yang and R. G. Parr, *Phys. Rev. B*, 1988, **37**, 785–789.
- 118 P. J. Stephens, F. J. Devlin, C. F. Chabalowski and M. J. Frisch, *J. Phys. Chem.*, 1994, **98**, 11623–11627.
- 119 C. Adamo and V. Barone, *J. Chem. Phys.*, 1999, **110**, 6158–6170.
- 120 J. P. Perdew, K. Burke and M. Ernzerhof, *Phys. Rev. Lett.*, 1996, **77**, 3865–3868.
- 121 M. M. Quintal, A. Karton, M. A. Iron, A. D. Boese and J. M. L. Martin, *J. Phys. Chem. A*, 2006, **110**, 709–716.
- 122 S. Grimme, *J. Phys. Chem. A*, 2005, **109**, 3067–3077.

ARTICLE

Journal Name

- 123 J. Tao, J. P. Perdew, V. N. Staroverov and G. E. Scuseria, *Phys. Rev. Lett.*, 2003, **91**, 146401.
- 124 S. Sinnecker, A. Rajendran, A. Klamt, M. Diedenhofen and F. Neese, *J. Phys. Chem. A*, 2006, **110**, 2235–2245.
- 125 M. Pavone, P. Cimino, O. Crescenzi, A. Sillanpää and V. Barone, *J. Phys. Chem. B*, 2007, **111**, 8928–8939.
- 126 Z. Rinkevicius, N. A. Murugan, J. Kongsted, K. Aidas, A. H. Steindal and H. Ågren, *J. Phys. Chem. B*, 2011, **115**, 4350–4358.
- 127 S. Kacprzak and M. Kaupp, *J. Phys. Chem. B*, 2006, **110**, 8158–8165.
- 128 S. M. Mattar, *J. Phys. Chem. B*, 2004, **108**, 9449–9455.
- 129 M. Witwicki and J. Jezierska, *Chem. Phys. Lett.*, 2010, **493**, 364–370.
- 130 M. Munzarová, in *Calculation of NMR and EPR Parameters. Theory and Applications*, eds. M. Kaupp, M. Bühl and V. G. Malkin, Wiley-VCH, Weinheim, First., 2004, pp. 463–482.
- 131 M. Munzarová and M. Kaupp, *J. Phys. Chem. A*, 1999, **103**, 9966–9983.
- 132 S. Kossmann, B. Kirchner and F. Neese, *Mol. Phys.*, 2007, **105**, 2049–2071.
- 133 J. Da Chai and M. Head-Gordon, *J. Chem. Phys.*, 2008, **128**, 084106.
- 134 S. Grimme, *J. Chem. Phys.*, 2006, **124**, 034108.
- 135 T. Schwabe and S. Grimme, *Phys. Chem. Chem. Phys.*, 2006, **8**, 4398.
- 136 S. Kozuch, D. Gruzman and J. M. L. Martin, *J. Phys. Chem. C*, 2010, **114**, 20801–20808.
- 137 D. G. Liakos, A. Hansen and F. Neese, *J. Chem. Theory Comput.*, 2011, **7**, 76–87.
- 138 D. G. Liakos and F. Neese, *J. Phys. Chem. A*, 2012, **116**, 4801–4816.
- 139 M. Sparta and F. Neese, *Chem. Soc. Rev.*, 2014, **43**, 5032–5041.
- 140 F. Neese, *J. Am. Chem. Soc.*, 2006, **128**, 10213–10222.
- 141 M. Kaupp, M. Bühl and V. G. Malkin, Eds., *Calculation of NMR and EPR Parameters. Theory and Applications*, Wiley-VCH, Weinheim, 2004.
- 142 R. Improta and V. Barone, *Chem. Rev.*, 2004, **104**, 1231–1254.
- 143 W. Kutzelnigg, U. Fleischer and M. Schindler, in *NMR Basic Principles and Progress*, Vol. 23, 1990, pp. 165–262.
- 144 G. L. Stoychev, A. A. Auer and F. Neese, *J. Chem. Theory Comput.*, 2017, **13**, 554–562.

View Article Online
DOI: 10.1039/D1CP01596F